



HAL
open science

Influence of Vertical Vibrations on the Stability of a Binary Mixture in a Horizontal Porous Layer Subjected to a Vertical Heat Flux.

Soumaya Ouadhani, Ali Abdennadher, Abdelkader Mojtabi, Alain Bergeon

► **To cite this version:**

Soumaya Ouadhani, Ali Abdennadher, Abdelkader Mojtabi, Alain Bergeon. Influence of Vertical Vibrations on the Stability of a Binary Mixture in a Horizontal Porous Layer Subjected to a Vertical Heat Flux.. *Transport in Porous Media*, 2018, 123 (372), pp.203-220. 10.1007/s11242-018-1059-5 . hal-03510693

HAL Id: hal-03510693

<https://hal.science/hal-03510693>

Submitted on 4 Jan 2022

HAL is a multi-disciplinary open access archive for the deposit and dissemination of scientific research documents, whether they are published or not. The documents may come from teaching and research institutions in France or abroad, or from public or private research centers.

L'archive ouverte pluridisciplinaire **HAL**, est destinée au dépôt et à la diffusion de documents scientifiques de niveau recherche, publiés ou non, émanant des établissements d'enseignement et de recherche français ou étrangers, des laboratoires publics ou privés.






Open Archive TOULOUSE Archive Ouverte (OATAO)

OATAO is an open access repository that collects the work of Toulouse researchers and makes it freely available over the web where possible.


This is an author-deposited version published in : <http://oatao.univ-toulouse.fr/Eprints>
ID : 19961

To link to this article : DOI:10.1007/s11242-018-1059-5
URL : <http://dx.doi.org/10.1007/s11242-018-1059-5>

To cite this version : Ouadhani, Soumaya  and Abdennadher, Ali and Mojtabi, Abdelkader  and Bergeon, Alain  *Influence of Vertical Vibrations on the Stability of a Binary Mixture in a Horizontal Porous Layer Subjected to a Vertical Heat Flux.* (2018) *Transport in Porous Media*, vol. 123 (n° 372). pp. 1-18. ISSN 0169-3913

Any correspondence concerning this service should be sent to the repository administrator: staff-oatao@listes-diff.inp-toulouse.fr

Influence of Vertical Vibrations on the Stability of a Binary Mixture in a Horizontal Porous Layer Subjected to a Vertical Heat Flux

Soumaya Ouadhani^{1,2} · Ali Abdennadher² ·
Abdelkader Mojtabi¹ · Alain Bergeon¹ 

Abstract We present an analytical and numerical stability analysis of Soret-driven convection in a porous cavity saturated by a binary fluid mixture and subjected to vertical high-frequency and small-amplitude vibrations. Two configurations have been considered and compared: an infinite horizontal layer and a bounded domain with a large aspect ratio. In both cases, the initial temperature gradient is produced by a constant uniform heat flux applied on the horizontal boundaries. A formulation using time-averaged equations is used. The linear stability of the equilibrium solution is carried out for various Soret separation ratios φ , vibrational Rayleigh numbers R_v , Lewis numbers Le and normalized porosity. For an infinite horizontal layer, the critical Rayleigh number Ra_c is determined analytically. For a steady bifurcation to a one-cell solution (the critical wavenumber is zero), we obtain $Ra_c = 12/(\varphi(Le + 1) + 1)$ for all R_v . When the bifurcation is a Hopf bifurcation or when the critical wavenumber is not zero, we use a Galerkin method to compute the critical values. Our study is completed by a nonlinear analysis of the bifurcation to one-cell solutions in an infinite horizontal layer that is compared to numerical simulations in bounded horizontal domains with large aspect ratio.

Keywords Porous media · Soret effect · Species separation · Vibrational convection

✉ Alain Bergeon
Alain.Bergeon@imft.fr

Soumaya Ouadhani
souadhan@imft.fr

Ali Abdennadher
ali.abdennadher@insat.rnu.tn

Abdelkader Mojtabi
mojtabi@imft.fr

¹ Institut de Mécanique des Fluides de Toulouse, IMFT, Université de Toulouse, CNRS, Toulouse, France

² Mathematical Engineering Laboratory, Tunisia Polytechnic School, University of Carthage, El Khaw-erzmi street, B.P.743, 2078 La Marsa, Tunisia

1 Introduction

Double-diffusive convection in a saturated porous medium due to temperature and concentration gradients has been widely studied because of its numerous fundamental and industrial applications. Reviews of recent developments and publications in this field can be found in reference Nield and Bejan (2013). Here, we study the effect of a mechanical high-frequency vibration on this thermosolutal convection with Soret effect in a saturated porous medium.

In a binary fluid mixture subjected to a temperature gradient, the Soret effect produces a species separation in the mixture. The mass flux \mathbf{J} takes into account both the isothermal diffusion and the thermodiffusion and reads:

$$\mathbf{J} = -\rho D \nabla C - \rho C_r (1 - C_r) D_T \nabla T, \quad (1)$$

where D is the mass diffusion coefficient, D_T is the thermodiffusion coefficient, ρ is the density, T is the temperature, C is the concentration of the denser species, C_r is the initial uniform concentration and $C_r(1 - C_r)$ is a weighting factor (Torres et al. 2013). Motivated by experiments in an oscillatory microgravity environment, the effects of mechanical vibrations on the stability of thermal systems have been the subject of numerous studies where the authors considered various directions, amplitudes and frequencies of the vibrations. In their book, Gershuni and Lyubimov (1998) presented a detailed review of the work done on the vibrational effects on convection in cavities including those filled with multi-component fluid mixtures.

Thermo-vibration problems in porous media have also received attention. Generally, these studies are classified in two groups: those concerning a porous medium saturated by a pure fluid and those in which the fluid is a binary mixture. Hereafter, we report only works dealing with high-frequency and small-amplitude vibrations; for other situations, the interested reader can refer to Razi et al. (2008). For the high-frequency and small-amplitude case, it is well established analytically that vertical vibrations have a stabilizing effect increasing the critical Rayleigh number. The work of Zen'kovskaya and Rogovenko (1999) extended earlier works by considering arbitrary directions of vibration. It shows that intense horizontal vibrations can destabilize the system giving rise to convection in situations that would normally be stable, such as in a zero gravity environment or in a fluid heated from above. Similarly, Govender (2005) showed for the case of vertical vibrations and a fluid heated from above (which is normally stable), the flow could be destabilized by gravity modulation due to vibrations. Using a time-averaged formulation, Bardan and Mojtabi (2000) reconsidered the case of vertical vibrations focusing on a horizontally bounded porous medium. In addition to performing linear stability analysis, they conducted a weakly nonlinear study and obtained analytically the solution as a function of the strength of vibration close to the onset of convection. They showed that increasing the vibration amplitude delays the onset of convection and may affect the nature of the first primary bifurcation. This work is extended by Bardan et al. (2004). The domain of validity of the mean flow formulation is discussed, and the authors show, using a weakly nonlinear stability analysis, that contrary to earlier published results, the first bifurcation is always supercritical.

All the papers cited above dealt with porous media saturated by a pure fluid. Double-diffusive convection caused by temperature and concentration gradients in a porous medium has also been widely studied due to its numerous fundamental and industrial applications. Some examples of interest are the migration of moisture in fibrous insulation, the transport of contaminants in saturated soil, drying processes and solute transfer in the mushy layer during the solidification of binary alloys. Soret-driven convective effects cannot be neglected in many of these situations. For the problems involving binary mixtures subjected to Soret

effect, Sovran et al. (2001) present a linear stability analysis of the horizontal infinite layer without vibrations. For a cell heated from below and for a positive separation ratio, they showed that the first primary bifurcation is a stationary one. Using a regular perturbation method in the case of long wave disturbances, they obtained the critical Rayleigh number. The same configuration is studied by Charrier-Mojtabi et al. (2004) who introduced high-frequency vibrations and investigated the problem for different aspect ratio and various directions of vibration. Their results demonstrate that for stationary and Hopf bifurcation, the vertical vibration has a stabilizing effect on the onset of convection while the horizontal vibration has a destabilizing effect. Elhajjar et al. (2009) revisited the problem, and their results suggest that vibrations could be used to improve the species separation in the case of the long wave mode. Furthermore, for the first time in this context, they performed a linear stability analysis of the long wave mode. They found that the one-cell solution loses stability via a Hopf bifurcation and that vibration had a stabilizing effect on it.

In the present paper, we use the formulation already used in Charrier-Mojtabi et al. (2004) and Elhajjar et al. (2009) of a shallow porous cavity saturated by a binary mixture subjected to the Soret effect. Motivated by applications of vibrations in thermogravitational columns (Nasrabadi et al. 2007), we focus on a large aspect ratio cavity filled with a porous medium and the limit of an infinite layer. We consider the case for which a vertical heat flux applied on the horizontal walls is responsible for the initial vertical temperature gradient whereas in the references Charrier-Mojtabi et al. (2004) and Elhajjar et al. (2009), the authors considered prescribed temperatures. Our thermal boundary conditions are close to those used by Yacine et al. (2016) for the same problem without vertical vibrations. Here, we show that vertical high-frequency and small-amplitude vibrations do not influence the stability of the base state when the Soret separation ratio is positive. This is an important difference with Charrier-Mojtabi et al. (2004) and Elhajjar et al. (2009). Moreover, we obtain analytical expressions for the steady bifurcation to one-cell solutions and propose a complete stability diagram.

In the next two sections, we present the mathematical formulation and the averaged equations. Following this, we next reconsider the linear stability analysis focusing on the one-cell solution. In the last sections, the linear and nonlinear analytical predictions are compared to direct numerical simulations.

2 Mathematical Model and Basic Equations

The configuration considered in this study is that of a horizontal porous layer of uniform thickness H , width L , permeability K^* and porosity ϵ^* , and which is filled with a binary mixture for which the Soret effect is taken into account. The origin of the coordinate system is located at the bottom of the porous cavity with x and z being the horizontal and vertical coordinates. All the boundaries are impermeable. We suppose that along the horizontal walls ($z = 0, H$) a uniform and constant heat flux per unit area q is applied while the vertical walls ($x = 0, L$) are assumed thermally insulated. We also assume that the porous medium is isotropic and homogeneous, that Darcy's law is valid, and that the Oberbeck–Boussinesq approximation is applicable: The thermophysical properties of the binary fluid are therefore considered to be constant except for the density in the buoyancy term, which is assumed to vary linearly with the local temperature T and concentration C :

$$\rho = \rho_r (1 - \beta_T (T - T_r) - \beta_C (C - C_r)), \quad (2)$$

where ρ_r is the fluid mixture density and where β_T and β_C are, respectively, the thermal and solutal expansion coefficients (the subscript r indicates reference values). When considering the reference frame related to the oscillating system, the gravitational field $\mathbf{g} = -g\mathbf{e}_z$ is replaced by: $\mathbf{g} + b\Omega^2 \sin(\Omega t)\mathbf{e}_z$, where Ω is the angular frequency of vibration, b is the displacement amplitude and t is the time.

The reference scales are H for length, $H^2/(k_p/(\rho c)_p)$ for time and κ/H for the velocity, where $\kappa = k_p/(\rho c)_f$ is the effective thermal diffusivity, k_p is the effective thermal conductivity of the saturated porous medium, $(\rho c)_p$ and $(\rho c)_f$ are the heat capacities of the saturated porous medium and of the fluid, respectively. Because of the applied heat flux, a temperature difference $\Delta T = qH/k_p$ is produced across the system and in response, the system develops a concentration difference $\Delta C = -\Delta T C_r(1 - C_r)D_T/D$ where D is the isothermal diffusion coefficient and D_T is the thermodiffusion coefficient. The dimensionless temperature and concentration are taken to be $(T - T_r)/\Delta T$ and $(C - C_r)/\Delta C$. In terms of the above definitions, the dimensionless governing equations are given by:

$$\nabla \cdot \mathbf{V} = 0, \quad (3)$$

$$B\partial_t \mathbf{V} + \mathbf{V} = -\nabla P + \text{Ra}(T + \varphi C)(1 - R \sin(\omega t)) \mathbf{e}_z, \quad (4)$$

$$\partial_t T + (\mathbf{V} \cdot \nabla) T = \nabla^2 T, \quad (5)$$

$$\epsilon \partial_t C + (\mathbf{V} \cdot \nabla) C = \text{Le}^{-1}(\nabla^2 C - \nabla^2 T). \quad (6)$$

Here, $\mathbf{V} = (u, w)$ is the dimensionless velocity field in (x, z) coordinates, P is the dimensionless pressure and T and C are now dimensionless temperature and concentration. The Rayleigh number Ra , the separation ratio φ , the Lewis number Le and the parameter R are defined by:

$$\text{Ra} = \frac{K^* g \beta_T H \Delta T}{\kappa \nu}, \quad \varphi = -C_r(1 - C_r) \frac{\beta_c D_T}{\beta_T D}, \quad \text{Le} = \frac{\kappa}{D}, \quad R = \frac{b\Omega^2}{g}, \quad (7)$$

where ν is the kinematic viscosity of the binary fluid. Additional parameters include the dimensionless frequency $\omega = \Omega H^2/(k_p/(\rho c)_p)$, the normalized dimensionless porosity $\epsilon = \epsilon^*(\rho c)_f/(\rho c)_p$ and the inverse Vadasz number $B = \text{Va}^{-1}$ defined by:

$$B \equiv \text{Va}^{-1} = \frac{\text{Da}(\rho c)_f}{\epsilon \text{Pr}(\rho c)_p}, \quad \text{Da} = \frac{K}{H^2}, \quad \text{Pr} = \frac{\nu}{\kappa}, \quad (8)$$

where Da is the Darcy number and Pr is the Prandtl number. In the dimensionless variables, the domain is $(x, z) \in \Gamma = [0, A] \times [0, 1]$ where $A = L/H$ is the aspect ratio. The dimensionless boundary conditions are:

$$z = 0, 1 : w = \partial_z T + 1 = \partial_z T - \partial_z C = 0, \quad (9)$$

$$x = 0, A : u = \partial_x T = \partial_x C = 0. \quad (10)$$

Figure 1 summarizes the geometry and boundary conditions. The term $B\partial \mathbf{V}/\partial t$ is usually neglected in the momentum equation since B is of order 10^{-6} . But in our problem, high-frequency vibrations cause very large accelerations and this term must be taken into account (Zen'kovskaya and Rogovenko 1999).

It should be mentioned that because of the Neumann boundary conditions for T and C , additional conditions must be specified to solve the equations. In particular, the mass flow rate through any vertical cross section should be zero and the species are also conserved in time:

$$\int_0^1 u(z) dz = 0, \quad \int_{\Gamma} C(z) d\Gamma = 0. \quad (11)$$

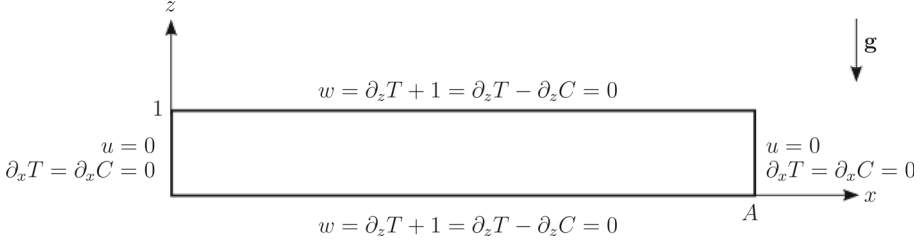


Fig. 1 Schematic view of the geometry with the dimensionless boundary conditions indicated

In the following, we will also consider an unbounded horizontal layer. In this case, the total heat and species transfer through any vertical cross section should be zero:

$$\int_0^1 (uT - \partial_x T) dz = \int_0^1 (uC - \partial_x (C - T)) dz = 0. \quad (12)$$

3 The Averaged Equations

In the limiting case of high-frequency and small-amplitude vibrations, the averaging method can be applied to study thermal vibrational convection (Charrier-Mojtabi et al. 2004; Razi et al. 2009; Elhajjar et al. 2009). According to this method, each field (\mathbf{V} , P , T , C) is written as the sum of two contributions. The first one, denoted by $(\bar{\mathbf{V}}, \bar{P}, \bar{T}, \bar{C})$, is the averaged field (the mean value calculated over the period $\tau = 2\pi/\omega$) and varies slowly with time (the characteristic time is large with respect to the period of the vibrations). The second one, denoted by $(\mathbf{V}', P', T', C')$, is the periodic rapidly varying part (the characteristic time is of the order of magnitude of the vibrational period). Writing:

$$(\mathbf{V}, P, T, C) = (\bar{\mathbf{V}}, \bar{P}, \bar{T}, \bar{C})(t) + (\mathbf{V}', P', T', C')(\omega t), \quad (13)$$

and using the high-frequency and low-amplitude hypothesis, the variables $(\mathbf{V}', P', T', C')$ can be expressed as functions of the averaged variables $(\bar{\mathbf{V}}, \bar{P}, \bar{T}, \bar{C})$ (Jounet and Bardan 2001). The details of the derivation and the theoretical justifications are presented in Simonenko and Zenkovskaya (1966), Simonenko (1972), Gershuni and Lyubimov (1998). We only mention here that the decoupling between the slow and rapidly varying fields requires introducing a Helmholtz decomposition of the averaged buoyancy term: $(\bar{T} + \varphi\bar{C})\mathbf{e}_z = \mathbf{H} + \nabla\xi$ where \mathbf{H} is the solenoidal part satisfying:

$$\nabla \cdot \mathbf{H} = 0, \quad \nabla \times (\bar{T} + \varphi\bar{C})\mathbf{e}_z = \nabla \times \mathbf{H}, \quad (14)$$

and $\mathbf{H} \cdot \mathbf{n} = 0$ on $\partial\Gamma$. The averaged equations read:

$$\nabla \cdot \bar{\mathbf{V}} = 0, \quad (15)$$

$$B\partial_t \bar{\mathbf{V}} + \bar{\mathbf{V}} = -\nabla \bar{P} + \left(\text{Ra}(\bar{T} + \varphi\bar{C}) + \text{Rv}((\mathbf{H} \cdot \nabla)\bar{T} + \frac{\varphi}{\epsilon}\mathbf{H} \cdot \nabla\bar{C}) \right) \mathbf{e}_z, \quad (16)$$

$$\partial_t \bar{T} + (\bar{\mathbf{V}} \cdot \nabla)\bar{T} = \nabla^2 \bar{T}, \quad (17)$$

$$\epsilon \partial_t \bar{C} + (\bar{\mathbf{V}} \cdot \nabla)\bar{C} = \text{Le}^{-1} (\nabla^2 \bar{C} - \nabla^2 \bar{T}), \quad (18)$$

with the boundary conditions (9,10) applied to the mean fields. The parameter $\text{Rv} = (\text{Ra}^2 R^2 B)/(2(B^2 \omega^2 + 1))$ is the modified vibrational Rayleigh number.

4 Linear Stability of the Equilibrium Solution in an Infinite Horizontal Porous Layer

The stability of the equilibrium solution of (15–18) was studied in Charrier-Mojtabi et al. (2004) in an infinite horizontal domain with prescribed temperatures along the horizontal boundaries. The authors restricted their work to the case $Le = 2$ for which the fluid is in the gaseous state. Here, we consider the situation in which the temperature difference is produced by a heat flux applied on the horizontal boundaries. We also consider the case of a high Lewis number, and we focus on the transition from the equilibrium solution to the mono-cellular flow. The conduction state:

$$\bar{\mathbf{V}}_0 = \mathbf{0}, \quad \bar{T}_0 = -z + cst, \quad \bar{C}_0 = -z + \frac{1}{2}, \quad \mathbf{H}_0 = \mathbf{0}, \quad (19)$$

is an equilibrium for all values of Ra . In order to investigate its stability, we introduce the stream-functions $\tilde{\Psi}$ and $\tilde{\Psi}_0$, respectively, associated to the velocity fields $\tilde{\mathbf{V}}$ and $\tilde{\mathbf{V}}_0$. Additionally, we define the solenoidal stream-functions $\tilde{\Psi}_s$ and $\tilde{\Psi}_{s_0}$, respectively, associated to $\tilde{\mathbf{H}}$ and $\tilde{\mathbf{H}}_0$. We look for normal modes and expand the variables as:

$$(\tilde{\Psi}, \tilde{T}, \tilde{C}, \tilde{\Psi}_s)(x, z, t) = (\tilde{\Psi}_0, \tilde{T}_0, \tilde{C}_0, \tilde{\Psi}_{s_0}) + (\tilde{\Psi}, \tilde{\theta}, \tilde{c}, \tilde{\Psi}_s)e^{\sigma t + ikx} + c.c. \quad (20)$$

where $\tilde{\Psi}_0 = 0$, $\tilde{\Psi}_{s_0} = 0$ and $(\tilde{\Psi}, \tilde{\theta}, \tilde{c}, \tilde{\Psi}_s)$ are complex functions of z . Note that even though the vibrations do not affect the base state (19), they may affect its stability and are therefore included in the perturbation expansion. We define $\tilde{\eta} = \tilde{c} - \tilde{\theta}$ and linearize equations (15–18) and (14) about the conduction state to get:

$$\begin{aligned} (B\sigma + 1)(D^2 - k^2)\tilde{\Psi} + \text{Ra}ik((1 + \varphi)\tilde{\theta} + \varphi\tilde{\eta}) - \text{Rv}\tilde{\Psi}_s k^2(1 + \frac{\varrho}{\epsilon}) &= 0, \\ (D^2 - k^2)\tilde{\theta} - \sigma\tilde{\theta} - ik\tilde{\Psi} &= 0, \\ \text{Le}^{-1}(D^2 - k^2)\tilde{\eta} - \epsilon\sigma(\tilde{\eta} + \tilde{\theta}) - ik\tilde{\Psi} &= 0, \\ (D^2 - k^2)\tilde{\Psi}_s + ik((1 + \varphi)\tilde{\theta} + \varphi\tilde{\eta}) &= 0, \end{aligned} \quad (21)$$

where $D = d/dz$. The boundary conditions now become:

$$z = 0, 1 : \tilde{\Psi} = \tilde{\Psi}_s = \partial_z \tilde{\theta} = \partial_z \tilde{\eta} = 0. \quad (22)$$

4.1 The Limiting Case of Long Wave Disturbances

In this part, we look for steady bifurcations. We study analytically the special case of the long wave mode. In some related studies in fluid media (Gershuni et al. 1997, 1999; Razi et al. 2008), the authors showed that asymptotic analysis results in a closed form relation for the stability threshold. In order to obtain such a relation, a regular perturbation method with the wavenumber as the small parameter is performed. We expand $(\tilde{\Psi}, \tilde{\theta}, \tilde{\eta}, \tilde{\Psi}_s, \sigma)$ as:

$$(\tilde{\Psi}, \tilde{\theta}, \tilde{\eta}, \tilde{\Psi}_s, \sigma) = \sum_{n=0}^{\infty} k^n (\tilde{\Psi}_n, \tilde{\theta}_n, \tilde{\eta}_n, \tilde{\Psi}_{s_n}, \sigma_n). \quad (23)$$

Substituting these expressions in Eqs. (21, 22) and separating the orders in k , we find a sequential system of equations. For the zeroth order (k^0):

$$\tilde{\Psi}_0 = 0, \quad \tilde{\Psi}_{s_0} = 0, \quad \tilde{\theta}_0 = cst, \quad \tilde{\eta}_0 = cst, \quad \sigma_0 = 0. \quad (24)$$

At order 1, we get:

$$\begin{aligned} \tilde{\Psi}_1 &= -\frac{i}{2} Ra (1 + \varphi(Le + 1)) \tilde{\theta}_0(z^2 - z), \quad \tilde{\Psi}_{s_1} = -\frac{i}{2} (1 + \varphi(Le + 1)) \tilde{\theta}_0(z^2 - z), \\ \tilde{\theta}_1 &= cst, \quad \tilde{\eta}_1 = cst, \quad \sigma_1 = 0, \end{aligned} \quad (25)$$

and at order 2:

$$\begin{aligned}\tilde{\Psi}_2''(z) &= -i\text{Ra} \left((1 + \varphi)\tilde{\theta}_1 + \varphi\tilde{\eta}_1 \right), \\ \tilde{\theta}_2''(z) &= i\tilde{\Psi}_1 + \tilde{\theta}_0(\sigma_2 + 1), \\ \tilde{\eta}_2''(z) &= i\text{Le}\tilde{\Psi}_1 + \tilde{\eta}_0, \\ \tilde{\Psi}_{s_2}''(z) &= -i \left((1 + \varphi)\tilde{\theta}_1 + \varphi\tilde{\eta}_1 \right),\end{aligned}\tag{26}$$

where '' is the second derivative with respect to z . After using the solvability condition, we find:

$$\sigma_2 = \frac{\text{Ra}}{12} (\varphi(\text{Le} + 1) + 1) - 1.\tag{27}$$

We note that σ_2 is real indicating that the conductive solution loses stability through a stationary bifurcation. For marginal stability, σ_2 is set equal to zero and we obtain the critical Rayleigh number:

$$\text{Ra}_c \equiv \frac{12}{1 + \varphi(\text{Le} + 1)}.\tag{28}$$

4.2 The General Case

The linear stability is investigated using a Galerkin method. The perturbations $(\tilde{\Psi}, \tilde{\theta}, \tilde{\eta}, \tilde{\Psi}_s)$ of the conduction state are expanded in series of polynomial functions satisfying all the boundary conditions:

$$\left\{ \begin{aligned}\tilde{\Psi} &= \sum_{n=1}^N a_n (1 - z) z^n \\ \tilde{\theta} &= b_1 + b_2 \left(z^2 - \frac{2}{3}z^3 \right) + \sum_{n=1}^N b_{n+2} (1 - z)^2 z^{n+1} \\ \tilde{\eta} &= c_1 + c_2 \left(z^2 - \frac{2}{3}z^3 \right) + \sum_{n=1}^N c_{n+2} (1 - z)^2 z^{n+1} \\ \tilde{\Psi}_s &= \sum_{n=1}^N e_n (1 - z) z^n\end{aligned}\right.\tag{29}$$

These expressions are introduced into system (21). The resulting algebraic system of equations has a non-trivial solution when its determinant is zero. In general, the determinant is complex. The procedure that we used to calculate the value of the critical Rayleigh number is the same as that described in Ouattara et al. (2012). Table 1 demonstrates its accuracy for $N = 5$.

For stationary bifurcations ($\sigma = 0$), the results obtained using a Galerkin method with $N = 4$ (with an accuracy of less than 1 %) indicate that:

$$0 \leq \text{Rv} \leq \text{Rv}_0 = \frac{640(\text{Le} + 1)}{7(\text{Le} - 1)^2}, \quad \text{Ra}_c = \frac{12}{1 + \varphi(\text{Le} + 1)}, \quad k_c = 0,\tag{30}$$

whereas for $\text{Rv} > \text{Rv}_0$, there exist φ_1, φ_2 roots of :

$$(\text{Le} + 1)\text{Rv}\varphi^2 + \frac{(3 + \text{Le})\text{Rv}}{2}\varphi + \frac{40}{7} + \frac{\text{Rv}}{2} = 0,\tag{31}$$

such that for φ in the interval of the two roots $[\varphi_1, \varphi_2]$, $k_c \neq 0$ (and therefore $\text{Ra}_c \neq 12/(1 + \varphi(\text{Le} + 1))$). It can be shown that $\varphi_2 < -1/(1 + \text{Le})$. We do not have analytical expressions for the critical wavenumber and Rayleigh number in this interval of φ . The

Table 1 Comparison between the exact values of the critical Rayleigh number associated to the first (i.e., lowest Ra) primary steady bifurcation when $k_c = 0$ to the values obtained using the Galerkin method at order 5 with $Le = 100$

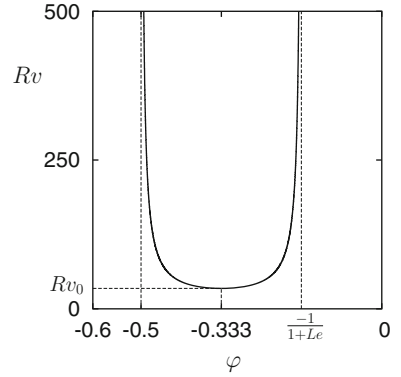
φ	Ra _c (Exact)	Ra _c (Galerkin)
-0.1	-1.319	-1.319
-0.05	-2.963	-2.963
0	12	12.000
0.1	1.081	1.081
0.2	0.566	0.566
0.5	0.233	0.233

Table 2 Critical wavenumber k_c and corresponding critical Rayleigh number Ra_c(k_c). The right column is the critical Rayleigh number Ra_c($k_c = 0$) (one-cell solution)

φ	k_c	Ra _c (k_c)	Ra _c ($k_c = 0$)
-0.2398	0	-27.347	-27.347
-0.26	0.931	-21.280	-21.428
-0.28	1.218	-17.290	-17.647
-0.30	1.374	-14.509	-15
-0.32	1.449	-12.516	-13.043
-0.34	1.459	-11.058	-11.538
-0.36	1.406	-9.973	-10.344
-0.38	1.280	-9.143	-9.37
-0.40	1.047	-8.476	-8.571
-0.4267	0	-7.691	-7.691

Parameters are $Le = 5$ and $Rv = 50$. As demonstrated by the table, the first (i.e., lowest Ra) primary bifurcation corresponds to a solution with $k_c \neq 0$ only when $\varphi \in [\varphi_1, \varphi_2]$ with $\varphi_1 \approx -0.4267$ and $\varphi_2 \approx -0.2398$. Resolution is $N = 4$

Fig. 2 Figure shows the variations with Rv of the interval $[\varphi_1, \varphi_2]$ (in the cup) in which the first (i.e., lowest Ra) primary bifurcation corresponds to $k_c \neq 0$. Calculations are carried out for $Le = 5$. The vertical asymptotes $\varphi = -0.5$ and $\varphi = -1/(1 + Le)$ are indicated in the figure. Writing $\varphi_1 = \varphi_2$ in Eq. (31) gives the coordinates of the minimum $\varphi \approx -0.333$. Relation (30) gives $Rv_0 \approx 34.28$



critical values are obtained with the Galerkin method (Ouattara et al. 2012). Table 2 shows the values obtained for $Le = 5$, $Rv = 50$. We get $\varphi_1 \approx -0.4267$, $\varphi_2 \approx -0.2399$ and a value of k_c varying from 0.931 to 1.459. Figure 2 shows the variations of φ_1 and φ_2 with Rv. The interval $[\varphi_1, \varphi_2]$ for which the first (i.e., lowest Ra) primary bifurcation corresponds to $k_c \neq 0$ is increasing with Rv but is contained in $[-0.5, -1/(1 + Le)]$ (see Fig. 2).

For the oscillatory instability ($\sigma = i\omega_H$, $\omega_H \neq 0$), the results are presented in Fig. 3 and Table 3. We used $N = 4$ with Le fixed and for different values of φ and Rv. We calculated the critical Rayleigh number Ra_c, the critical Hopf frequency ω_{Hc} and the associated critical wavenumber k_c . These results show that, for values of φ less than $-1/(Le + 1)$ and positive Ra, the conductive state loses stability through a Hopf bifurcation.

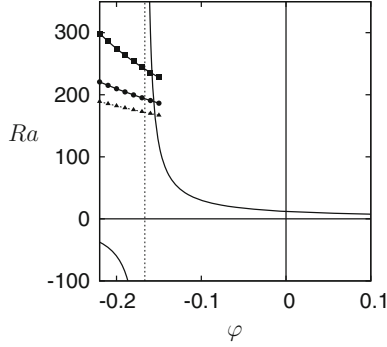


Fig. 3 Stability diagram for $Le = 5$, $Rv = 0$ and different normalized porosity values ϵ . The continuous line corresponds to the steady bifurcation to a one-cell structure for which the critical Rayleigh number does not depend on ϵ . The vertical dotted line corresponds to $\phi = -1/(Le + 1)$ and is a vertical asymptote for the steady bifurcation curves. The three other curves correspond to the Hopf bifurcation for $\epsilon = 0.5$ (squares), 0.7 (circles) and 0.9 (triangles). Each symbol corresponds to a value obtained with the Galerkin method at fourth order

Table 3 Critical Rayleigh numbers Ra_c , critical Hopf frequency ω_{H_c} and critical wavenumber k_c associated to the primary Hopf bifurcation for various ϕ , Rv and ϵ

ϕ	$Rv = 0$		$Rv = 10$	
	$\epsilon = 0.5$	$\epsilon = 0.7$	$\epsilon = 0.5$	$\epsilon = 0.7$
-0.16				
k_c	4.62	4.63	4.58	4.58
Ra_c	233.73	188.97	236.02	191.58
ω_{H_c}	19.49	16.73	19.25	16.47
-0.18				
k_c	4.61	4.63	4.58	4.58
Ra_c	251.40	198.00	253.55	200.51
ω_{H_c}	22.12	18.58	21.91	18.29
-0.20				
k_c	4.61	4.63	4.58	4.58
Ra_c	271.89	207.93	273.99	210.33
ω_{H_c}	24.89	20.42	24.66	20.10
-0.22				
k_c	4.60	4.63	4.58	4.59
Ra_c	296.29	218.90	298.15	221.20
ω_{H_c}	26.24	22.28	27.54	22.00

The results are obtained using the Galerkin method at order 6 with $Le = 5$

5 Analytical Solution of the Mono-cellular Flow

In the case of a shallow cavity ($A \gg 1$), we solve the full nonlinear problem analytically using the parallel flow approximation (Bennacer et al. 2003; Elhajjar et al. 2009). More precisely, we assume that the streamlines are parallel to the horizontal walls except in the vicinity of the vertical walls. So aside from these regions, the vertical component of the velocity can be neglected. The temperature and concentration are written as the sum of two terms: a first contribution corresponding to a linear longitudinal variation and a second contribution producing the transverse distribution. The solution can be written as follow:

$$\bar{\mathbf{V}} = \bar{u}(z) \mathbf{e}_x, \quad \bar{T} = m_T x + g(z), \quad \bar{C} = m_C x + h(z), \quad \mathbf{H} = h_s(z) \mathbf{e}_x, \quad (32)$$

where m_T and m_C are, respectively, the unknown constant temperature gradient and concentration gradient in the x direction. In the stationary case and using the boundary conditions, we obtain:

$$\bar{u}(z) = -f_0(2z - 1), \quad h_s(z) = -\frac{f_0}{\text{Ra}}(2z - 1), \quad (33)$$

and:

$$f_0 = \frac{1}{2} \text{Ra}(m_T + \varphi m_C), \quad (34)$$

$$g(z) = -\frac{1}{3} f_0 m_T z^3 + \frac{1}{2} f_0 m_T z^2 - z + cte, \quad (35)$$

$$h(z) = \frac{f_0(m_C \text{Le} + m_T)(6z^2 - 4z^3 - 1)}{12} + \frac{1 - m_C A}{2} - z, \quad (36)$$

$$m_T = \frac{5f_0}{f_0^2 + 30}, \quad m_C = -\frac{\text{Le} f_0(m_T f_0 - 5) - 30m_T}{\text{Le}^2 f_0^2 + 30}. \quad (37)$$

Replacing the expressions of m_T and m_C of (37) in Eq. (34) we obtain :

$$f_0 \left(\text{Le}^2 f_0^4 - \frac{5}{2} d_1 f_0^2 - \frac{25}{16} d_2 \right) = 0, \quad (38)$$

where:

$$d_1 = \text{Le}^2 \text{Ra} - 12\text{Le}^2 - 12, \quad d_2 = 48(\text{Ra}(1 + \varphi(\text{Le} + 1)) - 12). \quad (39)$$

The solutions of (38) are $f_0 = 0$ or:

$$f_0 = \pm \frac{\sqrt{5}}{2\text{Le}} \left(d_1 \pm \sqrt{d_1^2 + \text{Le}^2 d_2} \right)^{\frac{1}{2}}. \quad (40)$$

Of course, the number of solutions depends on the signs of $d_1^2 + \text{Le}^2 d_2$ and $d_1 \pm \sqrt{d_1^2 + \text{Le}^2 d_2}$ and these signs also depend on Ra at fixed Le and φ . But if a one-cell solution exists, there also exists another counter-rotating solution.

In the following, we focus on the configuration $\text{Ra} > 0$. It is clear that if $d_1^2 + \text{Le}^2 d_2 < 0$ no one-cell solution appears and we are left with the conduction state corresponding to $f_0 = 0$. Solving $d_1^2 + \text{Le}^2 d_2 = 0$ in terms of Ra gives two values $\text{Ra}_{2\pm}$:

$$\text{Ra} = \text{Ra}_{2\pm} \equiv \frac{12(\text{Le} + 1)}{\text{Le}^2} \left(\text{Le} - 2\varphi - 1 \pm 2\sqrt{\varphi(1 - \text{Le} + \varphi)} \right). \quad (41)$$

In between these two roots $d_1^2 + \text{Le}^2 d_2 < 0$. Therefore, $\text{Ra} < \text{Ra}_{2-}$ and $\text{Ra} > \text{Ra}_{2+}$ are necessary conditions for the existence of one-cell solutions. To ensure these solutions exist, we must have in addition at least one of this two conditions: $d_1 \pm \sqrt{d_1^2 + \text{Le}^2 d_2} > 0$ when $\text{Ra} = \text{Ra}_{2+}$. We calculated the expression φ_{sub} of φ below which this occurs:

$$\varphi_{\text{sub}} = -\frac{1}{1 + \text{Le} + \text{Le}^2 + \text{Le}^3}. \quad (42)$$

This Soret separation coefficient corresponds to the value below which the supercritical primary bifurcation to the one-cell solutions becomes subcritical. For $\text{Le} = 5$, it gives $\varphi_{\text{sub}} =$

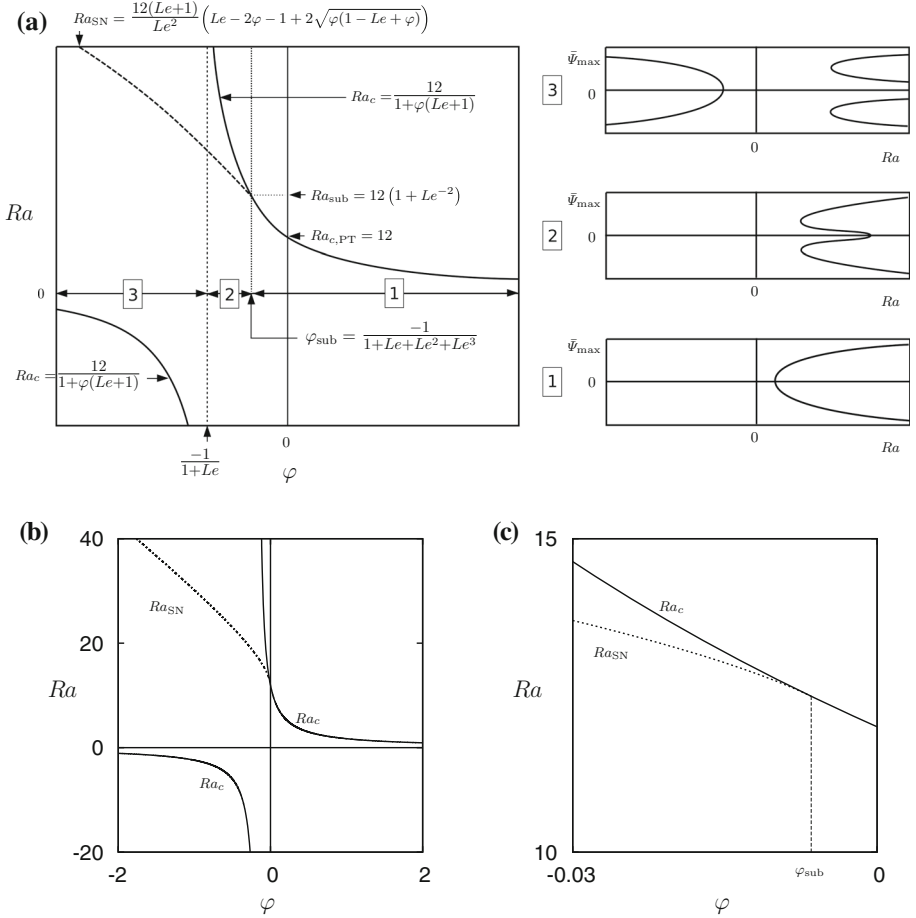


Fig. 4 **a** In the parameter space (φ, Ra) , the figure shows the stability diagram and the various analytical expressions obtained in the text. The figure is restricted to steady bifurcation points (primary bifurcations and saddle-nodes) associated to one-cell solutions. Three intervals of φ referred to as intervals 1, 2, 3 are identified. For φ chosen in an interval, the corresponding schematic bifurcation diagram reporting $\tilde{\psi}_{\max} = \pm \max_{\Gamma} |\tilde{\Psi}|$ as a function of Ra is shown on the right side of the figure. Interval 1 corresponds to $\varphi \in [\varphi_{\text{sub}}, +\infty)$, and the primary bifurcation is a supercritical pitchfork. The second interval corresponds to $\varphi \in [-1/(1+Le), \varphi_{\text{sub}}]$, and for φ chosen in this interval, the primary steady bifurcation is subcritical and associated to the existence of saddle-nodes. The last interval corresponds to $\varphi \in [-\infty, -1/(1+Le)]$. The primary steady bifurcation has disappeared for $Ra > 0$ and is replaced by a Hopf bifurcation not shown here (see Fig. 3). On the other hand, for $Ra < 0$, there exists a primary steady bifurcation. **b** shows the figure for $Le = 5$. **c** is a closer view of **b** showing in particular $\varphi_{\text{sub}} = -0.00641$ below which the primary bifurcation to one-cell solutions is subcritical

-0.00641 . When $\varphi < \varphi_{\text{sub}}$, the value $Ra_{\text{SN}} = Ra_{2+}$ corresponds to the saddle-node along the branch of one-cell solutions. It is also possible to obtain $\varphi_{\text{SN}} = \varphi(Ra_{\text{SN}})$:

$$\varphi_{\text{SN}} = -\frac{1}{48} \frac{(\text{Le}^2(Ra_{\text{SN}} - 12) + 12)^2}{\text{Le}^2 Ra_{\text{SN}} (\text{Le} + 1)}. \quad (43)$$

Figure 4a summarizes the various expressions obtained for the one-cell solution and shows the corresponding schematic bifurcation diagrams (restricted to steady states). Figure 4b, c

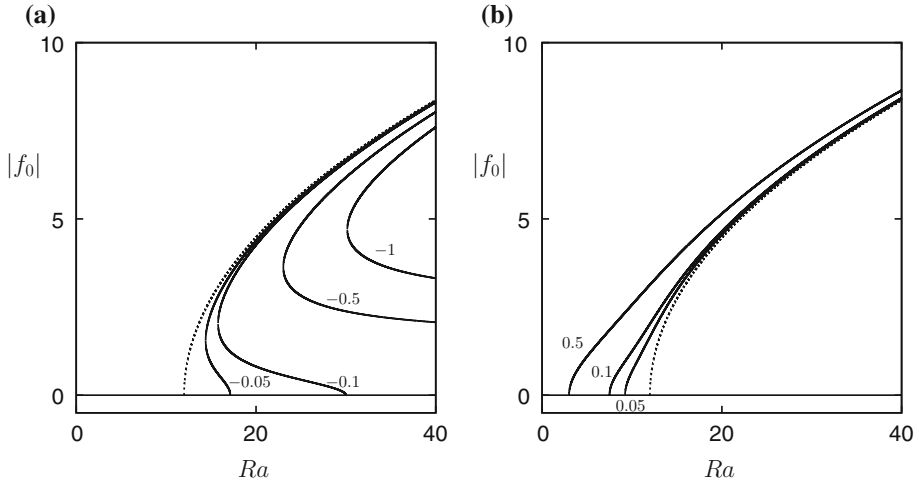


Fig. 5 a, b Bifurcation diagram showing $|f_0|$ (relation (40)) as a function of Ra for different values of φ indicated in the figures. The dashed line correspond to $\varphi = 0$. Parameters are $Le = 5$, $Rv = 0$. The domain is infinite in the horizontal direction

shows the stability diagram for $Le = 5$, and Fig. 5a, b shows the bifurcation diagram obtained with Eq. (40) when $Le = 5$ and $Ra > 0$. We identified three regions in the stability diagram of Fig. 4a. If $\varphi \in [\varphi_{\text{sub}}, +\infty)$, the primary bifurcation is a pitchfork. The corresponding bifurcation diagram is shown schematically on the right side of Fig. 4 and in Fig. 5b for various φ . If $\varphi \in [-1/(1+Le), \varphi_{\text{sub}}]$, the branch of one-cell solution bifurcates subcritically from the base state and turns around at larger amplitude via a saddle-node bifurcation at $Ra_{\text{SN}} < Ra_c$. This behavior is shown schematically on the right side of Fig. 4 and in Fig. 5a. Finally, for $\varphi \in [-\infty, -1/(1+Le)]$ the branches of one-cell solution are completely disconnected from the base state in the region $Ra > 0$ (see for instance Fig. 5a with $\varphi = -0.5$ or -1) whereas a supercritical bifurcation to one-cell solutions has appeared for $Ra_c < 0$. The analysis of this stability diagram and related bifurcation diagrams in the general context of binary fluid convection is conducted by Tuckerman (2001) using a low-dimensional dynamical system approach.

6 Numerical Simulations

We use a numerical continuation method to follow steady states emerging from small amplitude near the primary instability threshold to large amplitudes. Our numerical continuation method is based on a Newton solver for the time-independent version of the averaged equations and boundary conditions. The implementation of the method follows that of Mamun and Tuckerman (1995). The discretization in space is a spectral element method in which the domain is decomposed into n_e spectral elements of size $n_x \times n_z$. In each element, the fields are approximated by a high-order interpolant through the Gauss-Lobatto-Legendre points. The Newton solver uses a first-order time integration scheme for the equations. The diffusive linear part is treated implicitly, and the nonlinear part, explicitly. Since the latter requires the velocity, in the absence of vibrations, a Poisson problem is formulated for the stream-function and is solved subjected to Dirichlet boundary conditions. When $Rv = 0$,

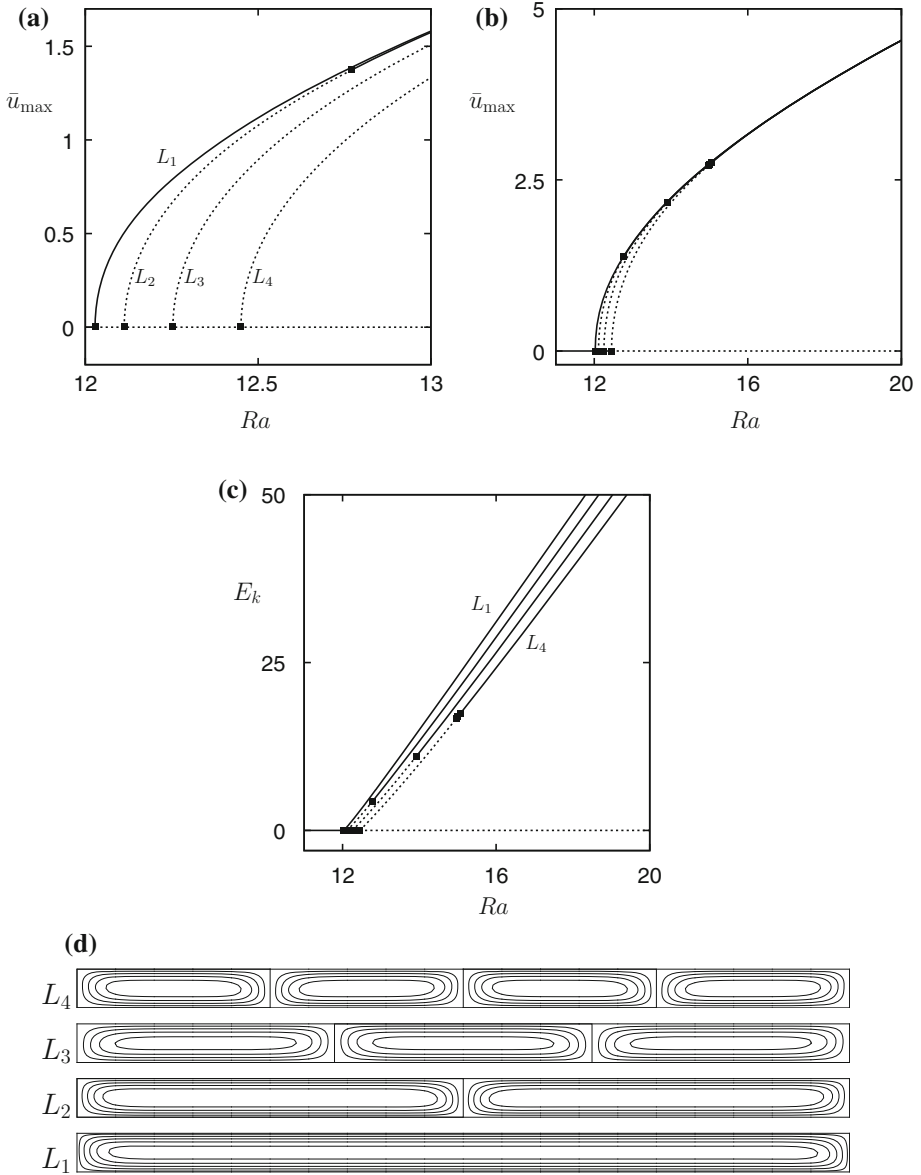


Fig. 6 **a** Bifurcation diagram showing the vicinity of the four first primary bifurcations from the conduction state in terms of the maximum horizontal component of the velocity \bar{u}_{\max} as a function of the Rayleigh number. Continuous (dashed) lines refer to linearly stable (unstable) solutions. Squares indicate primary and secondary bifurcation points. **b** same as **a** over a larger Rayleigh number interval. **c** same as **b** but in terms of the kinetic energy E_k as a function of the Rayleigh number. The secondary bifurcation along L_2 occurs at $Ra = 12.94$, and the successive secondary bifurcations along L_3 occur at $Ra = 13.93$ and 13.98 and along L_4 at $Ra = 14.96$, 15.0 and 15.05 . **d** Isovalues of the stream-function of the solutions at $Ra \approx 20$ along the branches L_n where n is the number of rolls. Parameters are $\varphi = 0$, $Rv = 0$ and $A = 20$

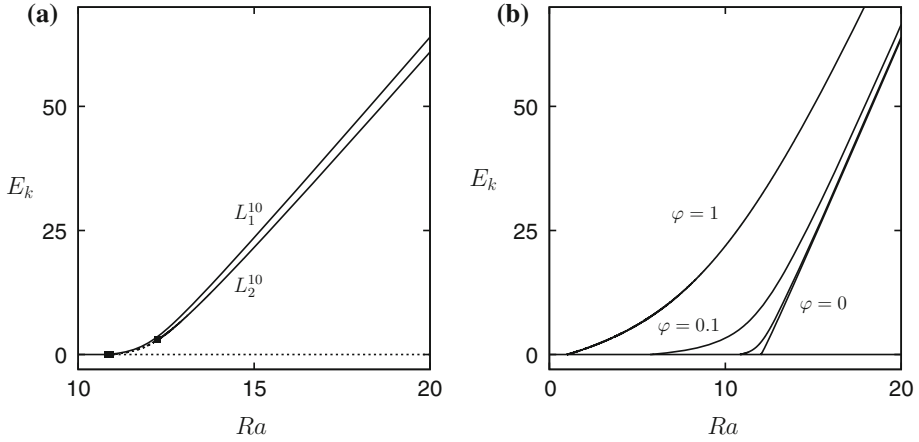


Fig. 7 **a** Bifurcation diagram showing the kinetic energy along the two first branches L_1^{Le} and L_2^{Le} bifurcating from the conduction state as a function of the Rayleigh number when $\varphi = 0.01$ and $Le = 10$. **b** Bifurcation diagram showing the kinetic energy along the first branch L_1^{10} bifurcating from the conduction state for $\varphi = 0, 0.01, 0.1$ and 1 . Other parameters are $Le = 10$, $Rv = 0$ and $A = 20$

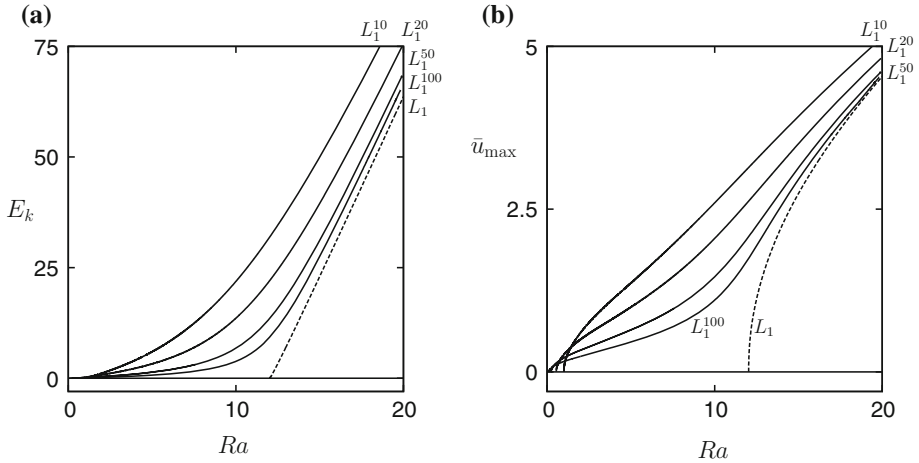


Fig. 8 Bifurcation diagram showing in **a** the kinetic energy and in **b** the maximum horizontal component of the velocity \bar{u}_{\max} as a function of the Rayleigh number along the first branch L_1^{Le} bifurcating from the conduction state for Lewis numbers $Le = 10, 20, 50, 100$ with $\varphi = 1$. The dashed line corresponds to L_1 (the fluid is not a binary mixture). Other parameters are $Rv = 0$ and $A = 20$

each timestep, therefore, requires the inversion of two Helmholtz problems and one Poisson problem. This is carried out using a Schur factorization procedure on the weak form of the equations. The linear stability of the solutions obtained during the continuation process is calculated using an Arnoldi method as described in Mamun and Tuckerman (1995). More details on the code and its adaptation to other physical problems can be found in Lo Jacono et al. (2011, 2013) and Beaume et al. (2013a,b).

We consider in this part a bounded domain. Since we also wish to compare the results for this geometry to those obtained for the infinite layer, we consider a large aspect ratio

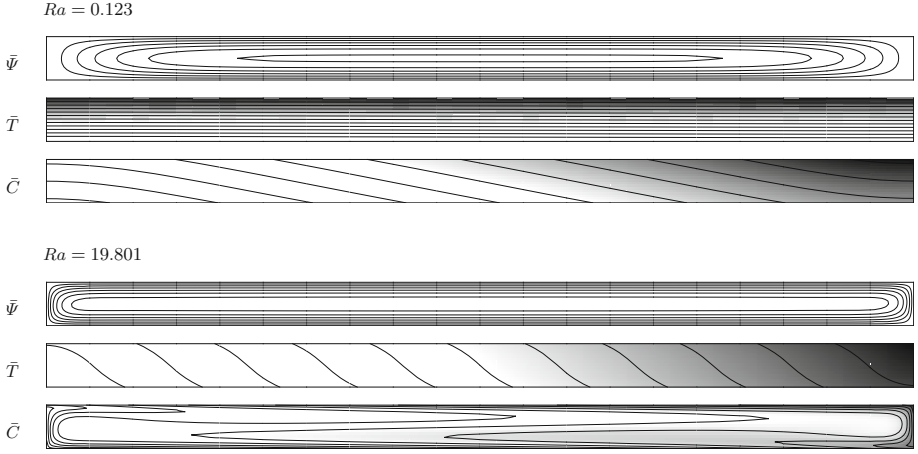


Fig. 9 Two solutions for two Rayleigh numbers: $Ra = 0.123$ which is close to the threshold and $Ra = 19.801$ which corresponds to a regime dominated by the thermally induced buoyancy force. The snapshots show the isovalues of the stream-function, temperature and concentration. The isovalues are equidistant between the minimum and maximum values. For \tilde{T} and \tilde{C} , 7 isovalues are drawn between $(\tilde{T}, \tilde{C})_{\min} = (-0.4, -2)$ and $(\tilde{T}, \tilde{C})_{\max} = (0.4, 2)$ for $Ra = 0.123$ and $(\tilde{T}, \tilde{C})_{\min} = (-4, -0.15)$ and $(\tilde{T}, \tilde{C})_{\max} = (4, 0.15)$ for $Ra = 19.801$. Parameters are $Le = 100$, $\varphi = 0.1$, $Rv = 0$ and $A = 20$

$A = 20$. All results are computed with $Rv = 0$, $B = 0$ and $\epsilon = 1$ for various Lewis numbers Le and Soret separation ratios φ . We used $n_e = 20$ spectral elements with a resolution in each element ranging from $n_x = n_z = 17$ for $Le = 10$ to $n_x = n_z = 31$ for $Le = 100$. Some results have been compared to those obtained with the COMSOL Multiphysics software (Comsol Inc 2012), and an excellent agreement was observed.

Figure 6 shows the bifurcation diagram in the pure thermal case corresponding to $\varphi = 0$. Figure 6a–c reports the variations with the Rayleigh number of the maximum of the horizontal velocity component and of the kinetic energy $E_k = (1/2) \int_{\Gamma} \tilde{\mathbf{V}}^2 d\Gamma$. The first four primary bifurcations are computed, and the emerging branches are referred as L_n where n is the number of cells of the associated solutions (Fig. 6d). The first one corresponds to the one-cell structure. It bifurcates supercritically and is stable over the computational domain. The other bifurcating branches L_n ($n > 1$) are $n - 1$ times unstable close to the threshold. But along each branch, $n - 1$ secondary bifurcations occur. As a consequence, all branches progressively regain stability to finally become linearly stable. This explains why in Fig. 6 we observe an interval of Rayleigh numbers where the four branches are linearly stable (note that along the branch L_2 the two secondary bifurcations are very close one another).

Figure 7a shows the bifurcation diagram when $\varphi = 0.01$. The figure indicates that the stabilization mechanism persists for the branch L_2 when $\varphi \neq 0$. We should mention that the stability of the solutions may be affected by the value of ϵ . But a complete study of this dependence is beyond the scope of this paper.

Hereafter, we only focus on the one-cell solution. Figure 7b shows the variations of the kinetic energy with the Rayleigh number for various Soret separation ratios φ . As expected, when φ increases the threshold decreases. The figure reveals that for small positive values of φ , the transition from low to large kinetic energy happens once the Rayleigh number exceeds the pure thermal threshold $Ra_{c,PT} = 12$. Beyond this value, the thermal and solutal contributions to the buoyancy force are both destabilizing. More precisely, if the Soret separation ratio is

not too large (between 0 and 10^{-2}), the thermal contribution is dominant as soon as Ra is larger than $Ra_{c,PT}$. This is clear in Fig. 7b where the bifurcating branch approaches the pure thermal branch ($\varphi = 0$, dashed curve) for $\varphi = 0.1$ and 0.01 . On the other hand, below $Ra_{c,PT}$, only the solutal part is responsible for the onset of convection and for small values of φ , it produces a very weak flow.

Figure 8 shows the bifurcation diagram of the one-cell solutions for positive Soret separation ratio $\varphi = 1$ and various Lewis numbers $Le = 10, 20, 50$ and 100 . The branches are labeled L_1^{Le} and are all linearly stable in the computational domain. These results show that the behavior identified in the previous paragraph for small Soret separation ratios and moderate Lewis numbers, also appears with large Soret separation ratios and large Lewis numbers. For $Le = 100$, Fig. 8 shows that the instability produces a weak convection regime close to the threshold followed by a more intense flow for Rayleigh numbers larger than the pure thermal threshold $Ra_{c,PT} = 12$. The physical reason is, however, slightly different than in the case of small Soret separation ratios. The flow is produced by the thermal and solutal gradients. When $Ra > Ra_{c,PT}$, and for large Lewis numbers, the concentration becomes almost constant everywhere forming boundary layers. The comparison of the two regimes $Ra < Ra_{c,PT}$ and $Ra > Ra_{c,PT}$ is illustrated in Fig. 9. The figure shows that when $Ra > Ra_{c,PT}$ the flow becomes driven mainly by the thermally induced buoyancy force.

7 Conclusion

We have conducted a numerical and analytical study of the onset of Soret-driven convection in an isotropic homogeneous porous medium saturated by a binary fluid mixture and subjected to vertical high-frequency and small-amplitude vibrations. Two configurations have been considered and compared: an infinite horizontal layer and a bounded domain with a large horizontal extension. In both cases, the initial temperature gradient is produced by a constant uniform heat flux applied on the horizontal boundaries. In response, the system develops a concentration difference adding a solutal contribution to the thermally induced buoyancy force. The relative effect of these two forces depends on the sign of the Soret separation ratio φ and the sign of the temperature difference between top and bottom (Ra can be positive or negative).

In the first part, we studied the influence of the sign of the Soret separation ratio φ and the influence of the (normalized) porosity on the onset of convection using an averaged formulation of the equations. A very good agreement was obtained between the analytical critical values and the values obtained with a Galerkin numerical procedure. For steady bifurcation, the threshold does not depend on the normalized porosity; this is not the case for Hopf bifurcations. The stability properties differ from the classical constant temperature Soret–Horton–Rogers–Lapwood problem for which the critical Rayleigh number associated to the onset of one-cell solution is equal to $12/(\varphi Le)$. Here, the steady bifurcation occurs for $Ra_c = 12/(\varphi(Le + 1) + 1)$ when $\varphi > -1/(1 + Le)$. More precisely, we demonstrated that the vibrations have no effect on the critical Rayleigh number Ra_c and critical wavenumber ($k_c = 0$) when $\varphi > -1/(1 + Le)$. But the vibrations have an effect on the Hopf bifurcation threshold (positive Ra_c and $\varphi < -1/(1 + Le)$) and on the steady bifurcation when $Ra_c < 0$ and $\varphi < -1/(1 + Le)$. The present configuration differs from that in which the initial temperature gradient is produced by prescribed temperatures along the horizontal boundaries (Elhajjar et al. 2009).

In the second part, direct numerical simulations were carried out in order to corroborate the results obtained with the linear stability analysis of the base state. More precisely, using a numerical continuation method, the results for a bounded domain with large aspect ratio were compared to an analytical approach carried out for an infinite horizontal domain and restricting the comparison to the one-cell structure. Despite expected differences close to the threshold, an excellent agreement was observed when the velocity in the vertical mid-plane of the domain is compared. Finally, we computed the bifurcation diagrams for various Soret separation ratios and various Lewis numbers restricting our study to steady states with a particular focus on the one-cell solution. Even though our results of Sect. 6 are obtained with $Rv = 0$, they are expected to capture the nonlinear behavior of the solutions when $Rv \approx 0$.

Acknowledgements The authors are grateful to CNES (Centre National d'Etudes Spatiales) for its financial support.

References

- Bardan, G., Mojtabi, A.: On the Horton–Rogers–Lapwood convective instability with vertical vibration. *Phys. Fluids* **12**, 1–9 (2000)
- Bardan, G., Razi, Y.P., Mojtabi, A.: Comments on the mean flow averaged model. *Phys. Fluids* **16**, 1–4 (2004)
- Beaume, C., Bergeon, A., Knobloch, E.: Convectons and secondary snaking in three-dimensional natural doubly diffusive convection. *Phys. Fluids* **25**, 024105 (2013a)
- Beaume, C., Bergeon, A., Kao, H.-C., Knobloch, E.: Convectons in a rotating fluid layer. *J. Fluid Mech.* **717**, 417–448 (2013b)
- Bennacer, R., Mahidjiba, A., Vasseur, P., Beji, H., Duval, R.: The soret effect on convection in a horizontal porous domain under cross temperature and concentration gradients. *Int. J. Numer. Methods Heat Fluid Flow* **13**, 199–215 (2003)
- Elhajjar, B., Mojtabi, A., Charrier-Mojtabi, M.-C.: Influence of vertical vibration on the separation of a binary mixture in a horizontal porous layer heated from below. *Int. J. Heat Mass Trans.* **52**, 165–172 (2009)
- Charrier-Mojtabi, M.-C., Razi, Y.P., Maliwan, K., Mojtabi, A.: Influence of vibrations on Soret-driven convection in porous media. *Numer. Heat Transf. A Appl.* **46**, 981–993 (2004)
- Comsol Inc.: *Comsol Multiphysics Reference Guide*, 4.3 edn (2012)
- Gershuni, G.Z., Kolesnikov, A.K., Legros, J.-C., Myznikova, B.I.: On the vibrational convective instability of a horizontal binary mixture layer with Soret effect. *J. Fluid Mech.* **330**, 251–269 (1997)
- Gershuni, G.Z., Lyubimov, D.V.: *Thermal Vibrational Convection*. Wiley, Hoboken (1998)
- Gershuni, G.Z., Kolesnikov, A.K., Legros, J.-C., Myznikova, B.I.: On the convective instability of a horizontal binary mixture layer with Soret effect under transversal high frequency vibration. *Int. J. Heat Mass Trans.* **42**, 547–553 (1999)
- Govender, S.: Destabilising a fluid saturated gravity modulated porous layer heated from above. *Transp. Porous Media* **59**, 215–225 (2005)
- Jounet, A., Bardan, G.: Onset of thermohaline convection in a rectangular porous cavity in the presence of vertical vibration. *Phys. Fluids* **13**, 3324 (2001)
- Lo Jacono, D., Bergeon, A., Knobloch, E.: Three-dimensional spatially localized binary fluid convection in a porous medium. *J. Fluid Mech.* **730**, R2 (2013)
- Lo Jacono, D., Bergeon, A., Knobloch, E.: Magneto-hydrodynamic convectons. *J. Fluid Mech.* **687**, 595–605 (2011)
- Mamun, C.K., Tuckerman, L.S.: Asymmetry and Hopf bifurcation in spherical Couette flow. *Phys. Fluids* **7**(1), 80–91 (1995)
- Nasrabadi, H., Hoteit, H., Firoozabadi, A.: An analysis of species separation in a thermogravitational column filled with a porous medium. *Transp. Porous Media* **67**, 47–486 (2007)
- Nield, D.A., Bejan, A.: *Convection in Porous Media*, 4th edn. Springer, New York (2013)
- Ouattara, B., Khouzam, A., Mojtabi, A., Charrier-Mojtabi, M.-C.: Analytical and numerical stability analysis of Soret driven convection in a horizontal porous layer: the effect of conducting bounding plates. *Fluid Dyn. Res.* **44**(3), 031415 (2012)
- Razi, Y.P., Charrier-Mojtabi, M.-C., Mojtabi, A.: Thermal vibrational convection in a porous media saturated by a pure or binary fluid. *Theory Appl. Transp. Porous Media* **22**, 149–179 (2008)

- Razi, Y.P., Charrier-Mojtabi, M.-C., Mojtabi, A.: A summary of new predictive high frequency thermo-vibrational models in porous media. *Transp. Porous Media* **77**(2), 207–228 (2009)
- Simonenko, I.B., Zenkovskaya, S.M.: Effect of high frequency vibration on convection initiation. *Izv. Akad. Nauk SSSR Mekh. Zhidk. Gaza* **1**, 51–55 (1966)
- Simonenko, I.B.: A justification of the averaging method for a problem of convection in a field of rapidly oscillating forces and for other parabolic equations. *Math. Sb.* **87**(2), 236–253 (1972)
- Sovran, O., Charrier-Mojtabi, M.-C., Mojtabi, A.: Onset on Soret-driven convection in an infinite porous layer. *CRAS Ser. IIB Mech.* **329**(4), 287–293 (2001)
- Torres, J.F., Komiya, A., Henry, D., Maruyama, S.: Measurement of Soret and Fickian diffusion coefficients by orthogonal phase-shifting interferometry and its application to protein aqueous solutions. *J. Chem. Phys.* **139**, 074203 (2013)
- Tuckerman, L.S.: Thermosolutal and binary fluid convection as a 2×2 matrix problem. *Physica D* **156**, 325–363 (2001)
- Yacine, L., Mojtabi, A., Bennacer, R., Khouzam, A.: Soret-driven convection and separation of binary mixtures in a horizontal porous cavity submitted to cross heat fluxes. *Int. J. Therm. Sci.* **104**, 29–38 (2016)
- Zen'kovskaya, S.M., Rogovenko, T.N.: Filtration convection in a high frequency vibration field. *J. Appl. Mech. Tech. Phys.* **40**, 379–385 (1999)